Operando XAS/XRD and Raman spectroscopic study of structural changes of the iron molybdate catalyst during selective oxidation of methanol

Dr. Abhijeet Gaur[a,b], Max Schumann[a,c], Dr. Kristian Viegaard Raun[c], Matthias Stehle[a], Dr. Pablo Beato[d], Prof. Anker Degn Jensen[c], Prof. Jan-Dierk Grunwaldt[a,b], Ass. Prof. Martin Høj[c,*]

[a]*Institute for Chemical Technology and Polymer Chemistry, Karlsruhe Institute of Technology (KIT), Karlsruhe, D-76131 (Germany).*

[b]*Institute of Catalysis Research and Technology, Karlsruhe Institute of Technology (KIT), Karlsruhe, D-76131 (Germany).*

[c]*Department of Chemical and Biochemical Engineering, Technical University of Denmark (DTU), Kgs. Lyngby, DK-2800 (Denmark).*

[d]*Haldor Topsøe A/S, 2800 Kgs. Lyngby, Denmark*

**E-mail: mh@kt.dtu.dk; Tel: +45 45252842*

ABSTRACT

The structural changes of an iron molybdate/molybdenum oxide (Mo/Fe = 2.0) catalyst for the selective oxidation of methanol to formaldehyde were studied using combined *operando* X-ray absorption spectroscopy (XAS) and X-ray diffraction (XRD) as well as *operando* Raman spectroscopy. Under operating conditions, the Mo K-edge XANES spectra showed a transition from a mixture of α-MoO_3 and $Fe_2(MoO_4)_3$ towards only $Fe_2(MoO_4)_3$. XRD and Raman spectroscopy also showed disappearance of the α-MoO_3 phase with time on stream. The results evidenced that the α-MoO_3 component evaporated completely, while the $Fe_2(MoO_4)_3$ component remained stable. This was linked to a decrease in catalytic activity. Further studies unraveled that the rate of α-MoO_3 evaporation increased with increasing MeOH concentration, decreasing O_2 concentration and increasing temperature. The simultaneous measurements of catalytic activity and spectroscopy allowed to derive a structure-activity relationship showing that α-MoO_3 evaporation needs to be prevented to optimize MoO_3-based catalysts for selective oxidation of methanol.

Keywords: Formaldehyde; Normalized difference edge analysis; Raman spectroscopy; Selective oxidation; X-ray

Graphical abstract

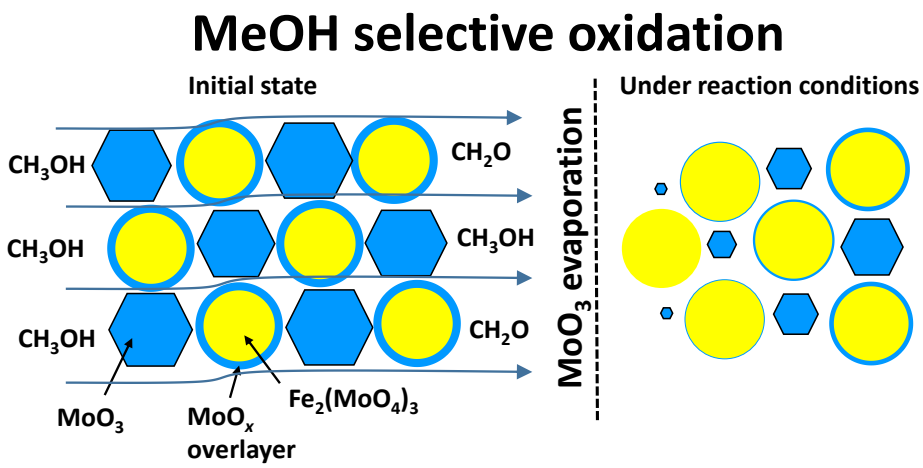

Table of content entry:

Structural changes of an iron molybdate/molybdenum oxide selective oxidation of methanol catalyst were studied using combined *operando* X-ray absorption spectroscopy (XAS) and X-ray diffraction (XRD) as well as *operando* Raman spectroscopy. α-MoO_3 formed volatiles species and evaporated during the initial time on stream while $Fe_2(MoO_4)_3$ remained stable. The rate of MoO_3 volatilization increased with increasing methanol concentration, decreasing oxygen concertation and increasing temperature.

1 INTRODUCTION

Formaldehyde is an important chemical intermediate in the production of a large number of industrial products including thermosetting resins, adhesives, paper, paints, synthetic fuel additives and fertilizers [1]. This underlines the importance of the industrial production of formaldehyde. The most effective industrial process in terms of yield and cost is the Formox process, which uses a bulk iron molybdate catalyst with an excess of molybdenum oxide ($Fe_2(MoO_4)_3/MoO_3$, denoted FeMo throughout the paper). It has been proposed that the excess MoO_3 primarily acts to replace molybdenum oxide lost through reaction with methanol, due to formation of volatile species at elevated temperatures, and to improve the selectivity, as iron oxide is known to catalyze the complete oxidation of methanol [2–5].

Understanding the molybdenum volatilization is important since it leads to early shutdown of industrial reactors, with subsequent cleaning and catalyst replacement. The main reason for the early shutdown is the increase in pressure drop caused by molybdenum oxide precipitating from the gas phase downstream in the reactor [6,7].

Although a number of structural studies, including *in situ* and *operando* studies, have been reported, they have mainly focused on the structure and interplay of the phases of the FeMo catalysts. For example, Yeo et al. [8] have reported recently that a surface layer of such FeMo catalysts is composed of octahedral Mo units, compared to the tetrahedral Mo centers found in $Fe_2(MoO_4)_3$. This over-layer structure has been proposed to be the active surface for the selective oxidation of methanol to formaldehyde.

Beale et al. [9] studied FeMo catalysts prepared by a hydrothermal method with Mo/Fe ratios ranging from the stoichiometric 1.5 to over-stoichiometric 3.0 using a number of characterization techniques including X-ray absorption spectroscopy (XAS), X-ray diffraction (XRD) and Raman spectroscopy. During calcination in air, the disappearance of a partly reduced Mo oxide (Mo_5O_{14}) phase and subsequent crystallization of the $Fe_2(MoO_4)_3$ phase was observed at around 300 °C. The study suggested

that the influence of calcination temperature and time on the catalytic activity is related to the growth of the MoO_3 particles.

In order to determine which factors affect the active species for methanol selective oxidation on iron molybdate catalysts, Brookes et al. [10–13] have studied this catalytic system extensively. It was concluded that selective oxidation of methanol depends on the presence of a molybdenum oxide dominated surface layer. In addition, the surface layer should have structural redox flexibility, i.e., the material must tolerate a degree of oxygen loss without permanent loss of structural integrity.

Soares et al. [14] also studied the deactivation of FeMo catalysts but only found significant deactivation of a stoichiometric catalyst, and ascribed this to formation of volatile Mo compounds with water and MeOH. They found that the XRD patterns of fresh and spent catalysts with excess Mo were similar, which might be due to low space velocity, resulting in complete MeOH conversion, and a significant part of the catalyst bed was exposed to a low concentration of MeOH.

O'Brien et al. [15–18] have studied the anaerobic dehydrogenation of methanol over MoO_3 by *in situ* wide angle X-ray scattering (WAXS), Raman spectroscopy and UV-vis spectroscopy. The study supported the Mars-van Krevelen mechanism and unraveled how the MoO_3 is reduced to MoO_2 through intermediate phases, probably $Mo_xO_yC_z$ and MoO_xH_y, which are likely oxy-methoxy and oxy-hydroxy compounds of molybdenum. These intermediates might be the volatile species or precursors to them [15,17]. The MoO_2 phase appeared to be stable, indicating that the Mo volatilization is more severe at industrial reaction conditions with oxygen in the gas phase [15]. Additional redox cycle experiments with iron molybdate (without excess of MoO_3) showed that $Fe_2(MoO_4)_3$ is reduced to $FeMoO_4$ and MoO_2 through formation of two intermediate phases: an oxygen defective intermediate pseudo-molybdate and a MoC phase [15,16]. The re-oxidation to $Fe_2(MoO_4)_3$ was slow and only partly reversible, possibly caused by the lack of excess MoO_3 [16].

The above studies indicate that there is a need for not only understanding the structure of the active site and the structural dynamics during redox cycling, but also the deactivation by molybdenum volatilization observed in industrial reactors near the inlet, where the MeOH concentration is high. Our group has studied the deactivation and degradation of a FeMo catalyst at about 400 °C, with Mo/Fe = 2.0 for up to 600 h on stream using a catalyst sieve fraction of 150 to 250 µm [19]. Operating at high space velocity, with significant MeOH concentration also at the outlet, the catalyst bed was uniformly deactivated. After 10 h on stream all excess MoO_3 was removed, after 100 h on stream the $Fe_2(MoO_4)_3$ was partly reduced to $FeMoO_4$ and after 600 h mainly $FeMoO_4$ and Fe_2O_3 remained. Additionally, the deactivation was studied using industrial catalyst pellets at 250-350 °C [20]. Inspection by scanning electron microscopy (SEM) showed that the volatilization of MoO_3 occurred from the outer pellet surface and formed a depletion layer where all MoO_3 had evaporated and a pellet core where the composition is like the fresh catalyst. Both the methanol oxidation reaction and the MoO_3 volatilization reaction were limited by internal diffusion in the pellets. The observed depletion layer moved gradually slower in a sharp front towards the center of the pellet.

Taking into account the findings from the above-mentioned studies, combined measurements of catalytic activity, oxidation state and phases present in the FeMo catalyst at industrially relevant conditions are needed for a structure-performance relationship. This is the objective of the present study and is important for rational improvement of the catalyst and optimization of the reaction conditions. By simultaneously measuring X-ray absorption near edge structure (XANES) and extended X-ray absorption fine structure (EXAFS) at the Mo K-edge, XRD, and the catalytic activity, we have obtained information about the oxidation states as well as the stability of all involved phases during the initial time on stream. *Operando* Raman spectroscopic studies have provided complementary evidence of the MoO_3 volatilization and its influence on the catalytic activity. The reaction is operated at high space velocity, in order to have uniform changes throughout the catalyst bed and to simulate conditions near the inlet of the industrial reactor where MoO_3 volatilization is most significant.

2 EXPERIMENTAL

2.1 CATALYST PREPARATION

The FeMo catalyst was prepared by a hydrothermal method with Mo/Fe ratio 2.0 as described in detail elsewhere [19]. For the *operando* XAS/XRD studies, the catalyst was calcined at 535 °C in air, subsequently crushed and ground with silica (Sigma-Aldrich) in a 1/5 catalyst/silica weight ratio. This mixture was pressed to form a pellet, crushed and sieved to 100-150 µm. For Raman spectroscopy, the catalyst was used as prepared from the hydrothermal synthesis. The dried precipitate was pressed to form a pellet, crushed and sieved to 150-300 µm and calcined at 400 °C in the Raman reaction cell.

2.2 *OPERANDO* XAS/XRD

Operando XAS measurements at the Mo K-edge (20.0 keV) in combination with XRD (25.13 keV) were carried out at BM31 of the Swiss-Norwegian beamlines (SNBL) at the European Synchrotron Radiation Facility (ESRF, Grenoble, France), operated at an energy of 6 GeV and with a current of 200 mA [21]. The beamline is designed in a flexible way to measure XAS and XRD or a combination of both techniques with fast switching between the XAS and the XRD monochromators. Three ionization chambers were used to detect the incident intensity (I_0), transmitted intensity (I_1), and reference Mo foil transmitted intensity (I_2). Mo K-edge XAFS was recorded from 19.8 to 21.0 keV in 1205 steps with 0.3 s acquisition per step, giving a total scan time of about 362 s. The ionization chambers were filled with pure N_2 at 1.445 bar (I_0) and 30 % Kr in N_2 at 1 bar (I_1 and I_2). For calibration and analysis purposes XAFS spectra of the references $Fe_2(MoO_4)_3$ (own synthesis, Mo/Fe = 1.5), MoO_3 (Merck), MoO_2 (Sigma Aldrich), FeO (Sigma Aldrich), Fe_2O_3 (Chem Pur), and Fe_3O_4 (Chem Pur) in the form of pellets were also recorded.

XAS spectra were analyzed with the software package IFEFFIT [22]. The spectra were energy calibrated, normalized, and background subtracted in Athena. EXAFS fittings were performed in Artemis

by using amplitude and backscattering factors obtained from model structures obtained from references of iron molybdate and molybdenum oxide [23,24]. XANES spectra were simulated using the computer code FEFF9 [25]. Further details about the data analysis are given in the Supplementary Information (Section 1).

XRD patterns were recorded with a CMOS-Dexela 2D detector at an X-ray wavelength of 0.4934 Å (25.13 keV). For each diffractogram, five bright and five dark images for background subtraction were recorded in the 2θ range of 2–35° with a data point spacing of approximately 0.01° and averaged. The sample to detector distance was calibrated with a LaB_6 reference. For XRD data treatment, the diffractograms were normalized to the most intense reflection of the SiO_2 dilutant, and a normalized diffractogram of only the SiO_2 dilutant measured at the same temperature was subtracted.

Two different monochromators were used for XAS and XRD, making the measurements quasi-simultaneous in the sense that XAS and XRD are measured subsequently with about 5 min for XAS, 1 min for XRD, and 1 min for each automatic monochromator change, giving a total cycle time of about 8 min.

Experiments were performed in a fixed-bed micro-reactor using 1 mm ID (0.01 mm wall thickness) quartz capillaries (Hilgenberg) [26]. 8-10 mg of the 100-150 µm sieve fraction catalyst/silica mixture was loaded and fixed by quartz wool, achieving a catalyst bed length of about 10 mm. The catalyst was heated with a gas blower (FMB Oxford) [27,28]. The total gas flow was 30 NmL/min and the desired gas mixture was achieved by mass flow controllers (Bronkhorst) mixing pure He, 20 % O_2/He and He saturated with MeOH by bubbling He through a MeOH reservoir at room temperature (22 °C). The tubes after the MeOH saturator and the outlet of the reactor until a formaldehyde precipitation flask were heat traced to avoid condensation of methanol, water and paraformaldehyde. The reactor outlet gas was analyzed using an OmniStar (Pfeiffer Vacuum) mass spectrometer measuring m/z = 4, 18, 29, 30, 31 and 32. The mass spectrometer data were normalized to the m/z = 4 trace as internal standard for a slow pressure increase in the MS during the MeOH exposure measurements. The m/z

= 29 trace was corrected for the MeOH contribution by subtracting the measured ratio to the *m*/*z* = 31 trace (ratio of *m*/*z* 29/31 = 0.807 for a MeOH/O_2/He gas mixture bypassing the reactor).

2.3 *Operando* Raman spectroscopy

Laser Raman spectroscopy (LRS) was performed using a confocal LabRam I microscope (Horiba, Jobin Yvon) equipped with a CVI Melles HeNe laser (633 nm at 25 mW max). A 10x objective was used to illuminate the sample in the reactor, resulting in a power of ca. 5 mW at the sample. Spectra were recorded averaging three acquisitions with an acquisition time of 120 s each and taken in a range from 100 to 1100 cm^{-1}. Continuous scans were recorded with a reduced acquisition time of 60 s, with decreased signal intensities. All spectra were baseline-subtracted.

Gas flows were set by mass flow controllers (MKS) and directed through a methanol container kept at 5 °C, which gives an approximate methanol concentration of 5 vol.%. The methanol container could also be by-passed. As described by Beato et al. [29], a commercially available Linkam CCR1000 catalyst reaction cell was modified to enable a fluidization-like movement of the catalyst particles by using an oscillating membrane pump, leading to temporarily reversed gas flow and upwards movement of the catalyst particles. This distributes the laser energy over all particles, circumventing local hot spots and sample changes caused by the high laser energy. In addition, it ensures uniform exposure of all catalyst particles to the reaction gas.

The reactor exit was linked to a T-piece, one way connected to a quadrupole mass spectrometer (Pfeiffer vacuum) and the other way connected to the membrane pump. Gas lines which connect the reactor and the mass spectrometer were heat traced to 200 °C in order to prevent precipitation of solid paraformaldehyde.

25 mg catalyst in the 150-300 µm sieve fraction was diluted with 18 mg Si and loaded in the steel reactor. The silicon band at 519 cm^{-1} was used as an internal standard for normalization of signal intensities and as an indicator for temperature induced shifts of Raman bands. The catalyst was calcined in

10 % O_2/N_2 for 2 h at 400 °C (total gas flow 40 NmL/min) and cooled to ambient temperature afterwards. Subsequently, the sample was heated to 375 °C and the gas flow was directed through methanol before entering the reaction cell, leading to a catalytic reaction atmosphere of approximately 5 % MeOH/9.5 % O_2/N_2. The catalyst was held on stream for 10 h.

3 Results and Discussion

3.1 Initial catalyst characterization by X-ray absorption spectroscopy

An iron molybdate/molybdenum oxide (FeMo) catalyst with overall Mo/Fe ratio = 2.0 was synthesized by a hydrothermal method and calcined at 535 °C, which resulted in an initial composition of a mixture of $Fe_2(MoO_4)_3$ and α-MoO_3 [19]. The Mo K-edge XANES spectrum of the initial state of the catalyst at 100 °C in 10 % O_2/He along with the XANES spectra of $Fe_2(MoO_4)_3$ and MoO_3 references are shown in Figure 1(a), with characteristic features A and B highlighted. Feature A at about 20006 eV is attributed to the dipole-forbidden/quadrupole-allowed 1s−4d transition associated primarily with tetrahedral geometry, but is also present with weak intensity in distorted octahedral geometry[30,31]. Feature B at about 20027 eV is assigned to the dipole-allowed 1s−5p transition and is a characteristic feature of Mo species with octahedral/distorted octahedral geometry [30,31]. The intensity of feature A in the sample is comparable to that of $Fe_2(MoO_4)_3$. However, the intensity of feature B is higher than for $Fe_2(MoO_4)_3$, showing that Mo is present in both tetrahedral (as in $Fe_2(MoO_4)_3$) as well as octahedral geometry (MoO_3 and surface MoO_x). As the initial state of the catalyst at 100 °C indicate mixed Mo(VI) phases, linear combination fitting (LCF) of the XANES spectrum was done using $Fe_2(MoO_4)_3$ and MoO_3 as standards (see Supplementary Information Figure S1), showing 21 % MoO_3 and 79 % $Fe_2(MoO_4)_3$. Since the fresh catalyst contained 17 wt.% α-MoO_3 and 83 wt.% $Fe_2(MoO_4)_3$ according to XRD [19], which corresponds to 22 mol.% of the Mo is bound as MoO_3 and 78 mol.% as $Fe_2(MoO_4)_3$, this is in reasonable agreement.

The corresponding k^3-weighted Fourier transformed EXAFS spectrum, along with the theoretical fit, is given in Figure 1(b). EXAFS fitting results are given in Table 1. The coordination number (CN) of the first Mo-O shell at 1.76 Å of 4.7 indicates tetrahedral nature of the Mo species due to the presence of $Fe_2(MoO_4)_3$. Mo-O shells at 2.04 and 2.36 Å indicate the additional presence of long axial Mo-O bonds due to the octahedral nature of the MoO_3 phase. Metal-metal Mo-Fe and Mo-Mo shells at 3.50 and 3.74 Å show the presence of both $Fe_2(MoO_4)_3$ and MoO_3. Thus, both XANES and EXAFS confirm the presence of MoO_3 and $Fe_2(MoO_4)_3$ in the initial state of the catalyst, as also found by *ex situ* XRD and reported previously [19]. Additionally, this was also confirmed by XRD measured at the beginning of the *operando* experiments (see Section 3.2.3).

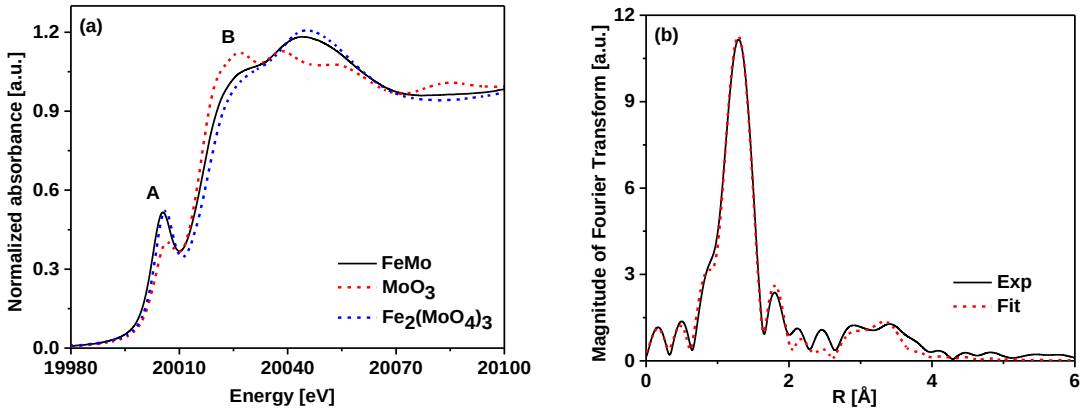

Figure 1: Normalized XANES (a) and k^3-weighted Fourier transformed EXAFS spectrum (b) of the initial state of the catalyst (FeMo) measured at 100 °C in a flow of 10 %O_2/He and the corresponding fit. The XANES spectra of MoO_3 and $Fe_2(MoO_4)_3$ are shown for comparison.

Table 1: EXAFS fitting results of the initial state of the catalyst measured at 100 °C shown in Figure 1(b), in comparison to the final state of the catalyst at 300 °C under operating conditions of 5 % MeOH/10 % O_2/He for 170 min. S_0^2 was fixed to 0.82(0.05) as determined from Mo foil.

	ΔE_0 = 2.8 (1.6), χ_v^2 = 82[a]			ΔE_0 = 2.0 (2.1), χ_v^2 = 75 [a]			
	Initial at 100 °C			Final at 300 °C			Phase
Path	R	CN	σ^2	R	CN	σ^2	
Mo-O_1	1.76	4.7±0.5	0.0038	1.77	5.4±0.5	0.0033	$Fe_2(MoO_4)_3$ and MoO_3
Mo-O_2	2.04/2.36	1/1	0.0085	2.04/2.36	1/1	0.0104	MoO_3
Mo-Fe	3.5	1	0.0055	Could not be fitted, weak signal.			$Fe_2(MoO_4)_3$
Mo-Mo	3.74	1	0.0055				MoO_3

[a] *χ_v^2 is the reduced chi-square goodness of fit parameter.*

3.2 Investigation of the structural changes during selective oxidation of methanol by *operando* XAS/XRD

The catalyst was in the next step heated under reaction conditions of 5 % MeOH/10 % O_2/He from 100 to 300 °C (at 10 °C/min) and kept at the final temperature of 300 °C to observe the structural changes. Figure 2(a) shows the normalized Mo K-edge XANES spectra under these conditions. The spectra do not show any shift towards lower energy of the edge position indicating that the oxidation state of Mo remained 6+ and, hence, no reduction was observed. The intensity of the pre-edge peak (feature A) was found to increase gradually and that of XANES feature B found to decrease (see Figure 2(b-c)). These changes indicate an increase in tetrahedral nature and a decrease in octahedral nature of the Mo centers, corresponding to decreasing MoO_3 content, because the geometry around the Mo atoms is octahedral in α-MoO_3 and distorted tetrahedral in $Fe_2(MoO_4)_3$ [32]. Initially, LCF analysis was applied to determine the variation in the contribution of different phases during the operando experiments. However, LCF fails when the observed changes in the features are very small. Hence, in such cases normalized difference edge analysis can be a useful tool, as discussed in Subsection 3.2.1.

Figure 2(d) shows the Fourier transformed EXAFS spectra where the amplitude of the first Mo-O shell increased under reaction conditions at 300 °C. Comparison of the structural parameters obtained from EXAFS fitting of the first and last spectra under reaction conditions is given in Table 1. For the last spectrum under operating conditions at 300 °C, the Mo-O CN at 1.77 Å, typical distance for tetrahedral Mo-O, shows significant increase, which indicates a transition towards tetrahedral coordination. The corresponding fitting in R space is given in the Supplementary Information (Figure S1).

Brookes et al. [11] also performed *in situ* XANES at the Mo K-edge on a catalyst consisting of six monolayers of MoO_x on the surface of an iron oxide core. However, for up to 120 min on stream at 250 °C in a flow of MeOH/O_2/He no apparent changes in the XANES spectra were observed. This is likely due

to the different type of catalyst with only a surface layer of MoO_x and the lower temperature, which limits the loss of MoO_x.

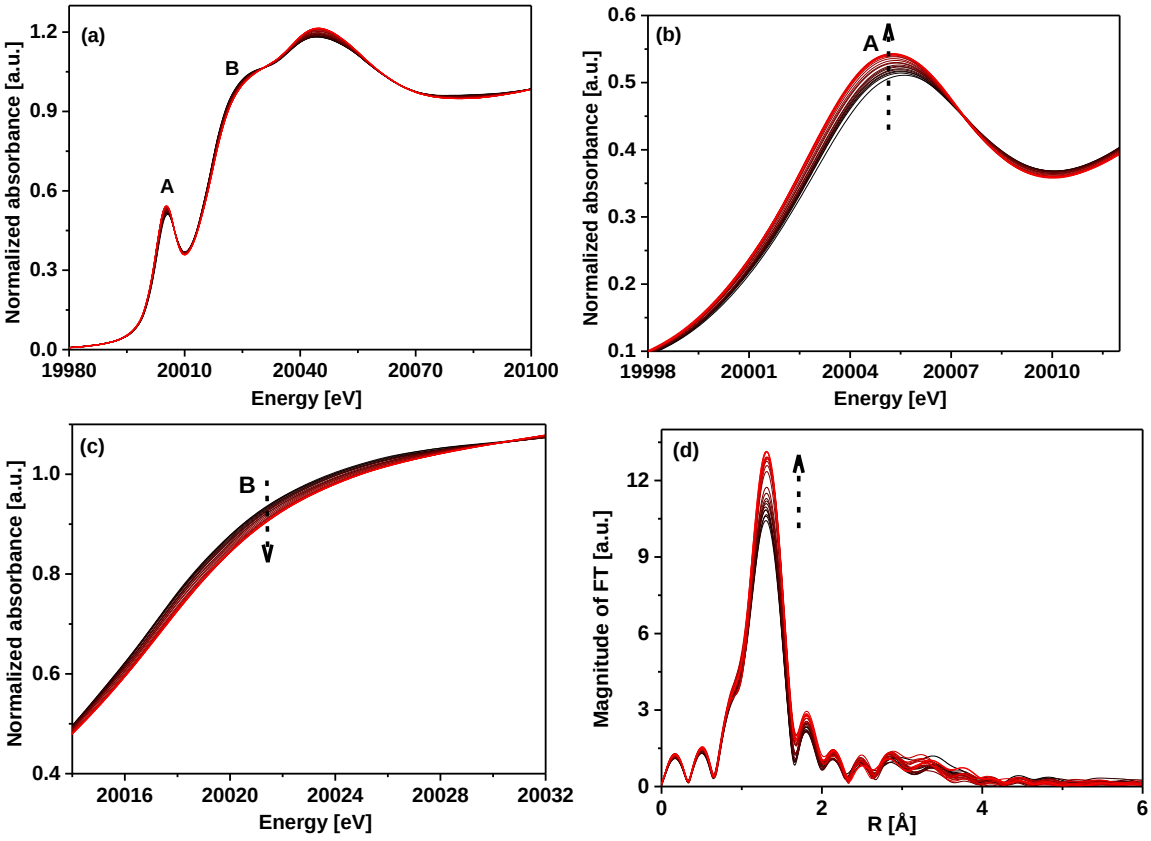

Figure 2: Operando Mo K-edge XANES spectra (a) and k^3-weighted Fourier transformed EXAFS spectra (d) of the FeMo catalyst under reaction conditions at 300 °C and 5 % MeOH/10 % O_2/He. Changes in the coordination geometry of the Mo atoms indicated by the change in intensity of XANES features A (b) and B (c).

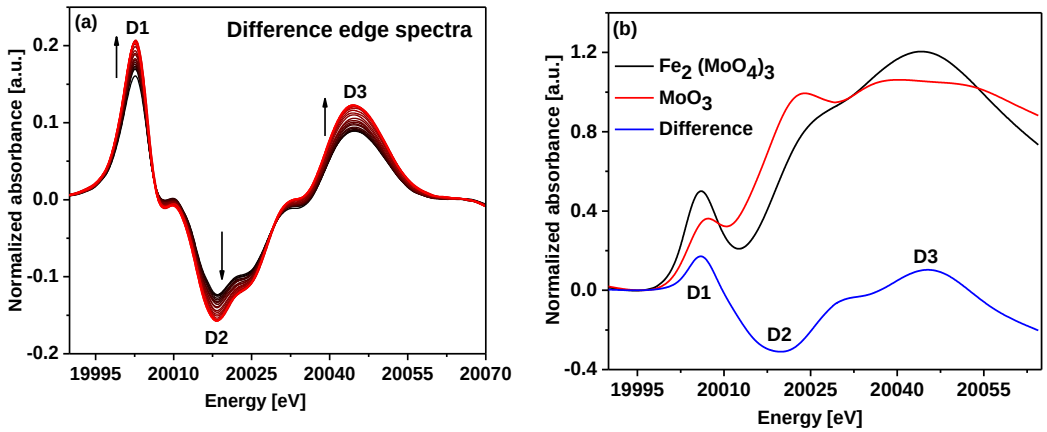

Figure 3: (a) Difference spectra obtained by subtracting an experimental XANES spectrum of an α-MoO_3 reference from each spectrum shown in Figure 2(a) with characteristic features D1, D2 and D3 highlighted. (b) Calculated $Fe_2(MoO_4)_3$ and MoO_3 XANES spectra and the corresponding difference spectrum.

3.2.1 Normalized difference edge analysis

In order to quantify the decrease of octahedral Mo species, i.e. the decrease of the MoO_3 content, the method of normalized difference edge analysis was used [33,34]. The experimental XANES spectrum of an α-MoO_3 reference was subtracted from each of the spectra obtained at 300 °C under reaction conditions (shown in Figure 2(a)). This gives a particularly shaped spectrum (similar to the shape of first derivative spectrum) as shown in Figure 3(a) with positive and negative peaks at characteristic energies marked D1, D2 and D3. In order to verify the origin of these features, XANES spectra of $Fe_2(MoO_4)_3$ and MoO_3 were simulated with the computer code FEFF9 using the available crystallographic data of these compounds [23,24]. Feff.inp files generated using the program Artemis are given in the Supplementary Information (Section 1). The simulated spectra and the corresponding difference spectrum are shown in Figure 3(b). The simulated spectra are not corrected for the edge energy and are shown as obtained from FEFF9. Therefore, the features are located at slightly different energies compared to the features obtained from the experimental spectra (Figure 3(a)), which are calibrated using a Mo foil.

Using the additive nature of the absorption spectra from each species in the sample [34], the intensities of features observed in the XANES spectra under operating conditions can be correlated to the contribution from MoO_3 and $Fe_2(MoO_4)_3$ using linear combination analysis. XANES spectra were calculated with 10 % to 1 % contribution from MoO_3 and 90 to 99 % from $Fe_2(MoO_4)_3$, shown in Figure 4(a). The difference spectra shown in Figure 4(b) are obtained by subtracting the simulated MoO_3 spectrum from the linear combined XANES spectra. The difference spectra show variation in the intensities of the characteristic peaks D1, D2 and D3, which, when plotted as function of the percentage of MoO_3, show a linear correlation between these parameters (Figure 5). Hence, changes in intensities of the features observed in the difference spectra correspond to changes in the ratio between $Fe_2(MoO_4)_3$ and MoO_3. A change of 1 %-point of MoO_3 corresponds to a change of intensity of 0.00152 for feature D3, measured as the negative slope of the D3 curve in Figure 5. Since the fresh

catalyst had 22 mol.% of the Mo bound as MoO_3 and 78 mol.% as $Fe_2(MoO_4)_3$, the total change in D3 after complete evaporation of all MoO_3 is expected to be 0.0335.

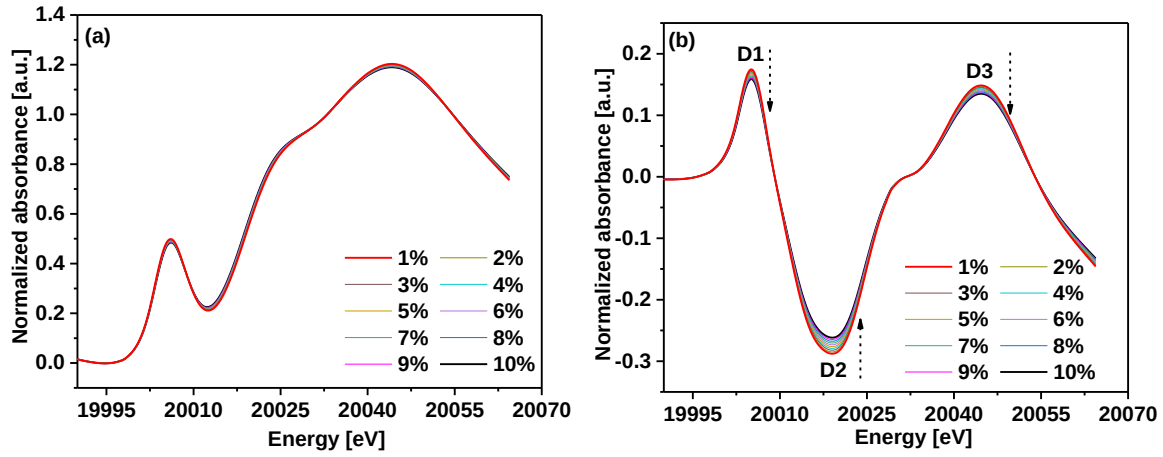

Figure 4: (a) Calculated XANES spectra of mixtures of $Fe_2(MoO_4)_3$ and MoO_3 with increasing fraction of MoO_3. (b) Difference spectra of the spectra in (a) and the calculated spectrum of MoO_3 showing characteristic changes of features D1, D2 and D3.

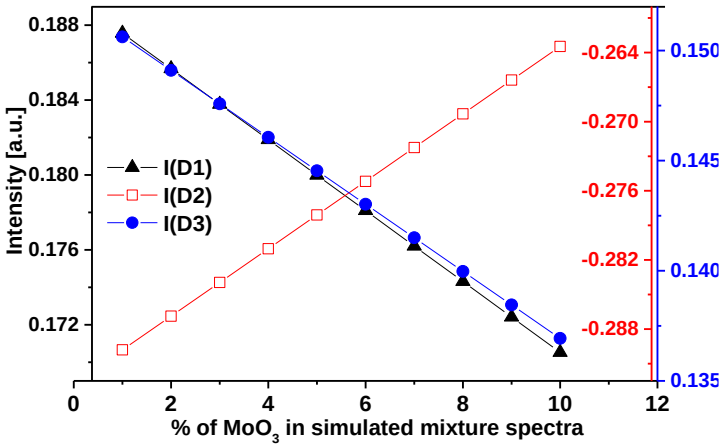

Figure 5: Intensities of characteristic features D1, D2 and D3 in the difference spectra from Figure 4(b) as function of the MoO_3 percentage in mixtures of $Fe_2(MoO_4)_3$ and MoO_3.

Figure 6 shows the variation in the intensities of features D1, D2 and D3 as function of time on stream for the catalyst exposed to 300 °C under reaction conditions of 5 % MeOH/10 % O_2/He (the corresponding difference spectra are shown in Figure 3(a)). During the first 20 min the sample is heated from 100 to 300 °C at 10 °C/min, after which the temperature is constant. The observed increase in intensity of features D1 and D3 and corresponding decrease in feature D2 demonstrates that the contribution from MoO_3 continuously decreased under these conditions, i.e. that MoO_3 evaporates. After 110 to 120 min on stream, the intensities became almost constant and the total

intensity change of feature D3 was 0.0332, which is very close to the theoretically calculated total change of 0.0335, indicating that all MoO_3 had evaporated. This is qualitatively in agreement with previous *ex situ* laboratory experiments, except that the total evaporation of the MoO_3 took about 10 h in the laboratory reactor [19]. However, the conditions in the *operando* experiments favored evaporation due to the very small particle size and higher space velocity in the *operando* experiments, resulting in lower conversion and higher average MeOH concentration throughout the catalyst bed.

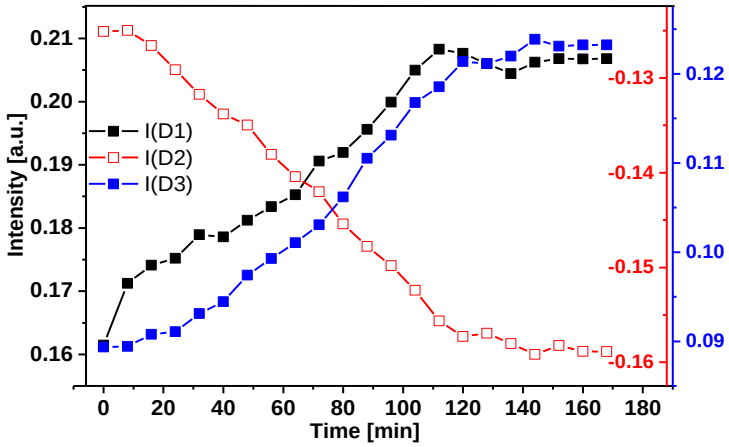

Figure 6: Intensities of characteristic features D1, D2 and D3 (c.f. Fig.3(a)) as function of time on stream at 300 °C and 5 % MeOH/10 % O_2/He. The increase in I(D1) and I(D3) and corresponding decrease in I(D2) shows evaporation of MoO_3 and after 120 min all MoO_3 has evaporated. During the first 20 min the sample is heated from 100 to 300 °C after which it is isothermal.

3.2.2 Catalytic activity with decreasing MoO_3 content

The catalytic activity and the intensity of feature D3 is shown in Figure 7 for a reaction gas composition of 5 % MeOH/10 % O_2/He. Initially, as the sample was heated from 100 to 300 °C the concentration of MeOH decreased and correspondingly the concentrations of water and formaldehyde increased. With time on stream, the concentration of MeOH started to increase again and water and formaldehyde decreased, confirming the *ex situ* laboratory observations that the evaporation of the MoO_3 leads to a decrease in catalytic activity [19].

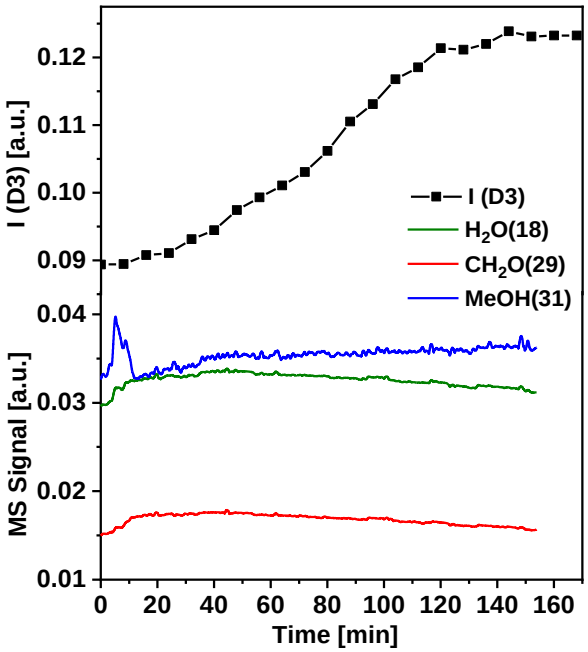

Figure 7: Intensity of feature D3 as function of time with MS traces overlaid for operando conditions of 300 °C (first 20 min. are heat up from 100 to 300 °C at 10 °C/min) at gas composition 5 % MeOH/10 % O_2/He.

Additional *operando* experiments were performed using more severe reaction conditions of lower oxygen concentration (5 % MeOH/5 % O_2/He) as well as higher MeOH concentration (9.5 % MeOH/5 % O_2/He) both conducted at 300 °C (given in Figures S3 and S4 in the Supplementary Information). The trends in MeOH, H_2O, and formaldehyde concentrations as well as the intensity of the difference feature D3 were the same as for the base case experiment (see Supplementary Information Figures S5(a) and (b)). However, the rate of the changes was higher. The rates of change in intensity of feature D3, along with the total intensity change, are summarized in Table 2. This shows that decreasing the O_2 concentration from 10 to 5 % increased the rate of MoO_3 evaporation by approximately 67 % and additionally increasing the MeOH concentration from 5 to 9.5 % (at 5 % O_2) further increased the rate by a factor 2. The total change in intensity of feature D3 was approximately the same for all conditions, similar to or slightly higher than the theoretically calculated value of 0.0335, indicating that complete MoO_3 evaporation occurred at all conditions.

Table 2: Rate of intensity change of feature D3, corresponding to rate of MoO_3 evaporation, measured as the slope in the linear region, at 300 °C under different gas compositions.

Conditions	Rate [min^{-1}]	Total intensity change
5 % MeOH/10 % O_2/He	$0.33 \cdot 10^{-3}$	0.0332
5 % MeOH/5 % O_2/He	$0.55 \cdot 10^{-3}$	0.0352
9.5 % MeOH/5 % O_2/He	$1.1 \cdot 10^{-3}$	0.0347

3.2.3 *Operando* XRD

Using the unique setup at BM31 (SNBL, ESRF), Mo K-edge XAS and XRD could be measured after each other with a cycle time of about 8 min. The acquired *operando* diffractograms of the FeMo catalyst at 300 °C and 5 % MeOH/10 % O_2/He are shown in Figure 8(a). Most reflections observed belong to $Fe_2(MoO_4)_3$, with its most intense peak at 7.32° and other significant single or overlapping, non-resolved reflections at 6.93, 7.55-7.63, 7.92, 8.16, 8.73-8.82° (ICSD collection code 100606). Initially, the sample was heated from 100 to 300 °C at 10 °C/min, which resulted in minor peak shifts to lower diffraction angles. α-MoO_3 was also observed by the reflections at 7.43, 8.16-8.23 and 8.67° (ICSD 151751), but they partly overlap with the reflections of $Fe_2(MoO_4)_3$ at 7.32, 7.55-7.63, 8.16, and 8.73-8.82° respectively. Between 8.25 and 8.55°, two glitches belonging to the background subtraction of the silica dilutant can be seen. The observed intensity decrease with time on stream of the reflections belonging to MoO_3 and the final stabilization of the diffractogram clearly shows the disappearance of α-MoO_3. Together with the by XAS observed transition towards more tetrahedral coordination geometry and that Mo^{6+} is not reduced, the disappearance of the α-MoO_3 reflections confirms the evaporation of MoO_3. Additionally, no reflections belonging to the reduced phases $FeMoO_4$ or MoO_2 were observed. The most intense reflections of $FeMoO_4$ are expected at 8.04 and 8.94° (ICSD 43012) and the most intense reflection of MoO_2 is expected at 8.26° (ICSD 24322), which overlaps the $Fe_2(MoO_4)_3$ reflections and the glitches, so a significant degree of reduction must be achieved before these phases would be clearly observed, considering the resolution of the *operando* XRD.

Similar *operando* XRD results at 300 °C acquired for gas compositions of 5 % MeOH/5 % O_2/He and 9.5 % MeOH/5 % O_2/He are given in the Supplementary Information (Figures S6 (a) and (b)). They

show qualitatively the same behavior, but the rate of disappearance of the α-MoO_3 reflections was higher.

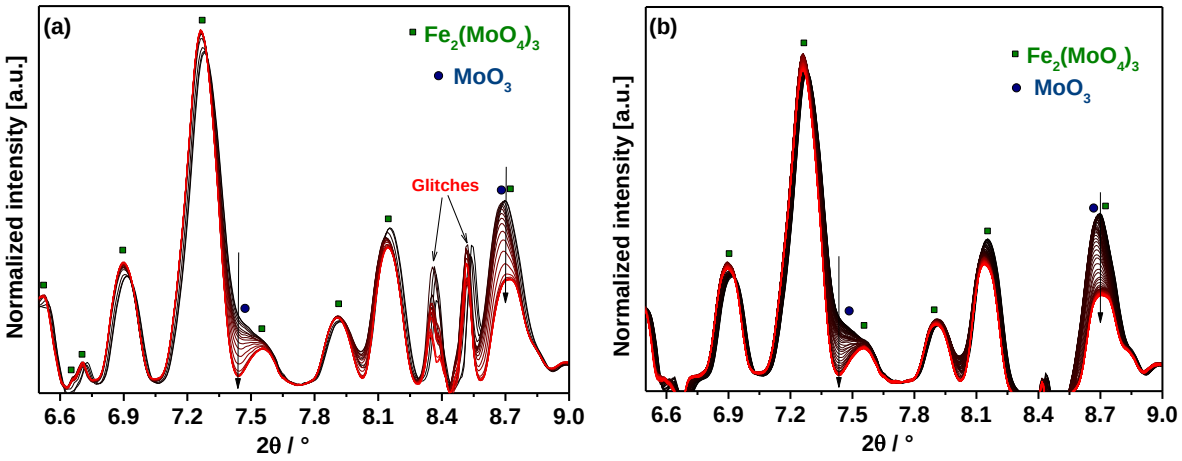

Figure 8: Operando XRD (E = 25.13 keV, λ = 0.4934 Å) at (a) 300 °C and (b) 350 °C under 5 % MeOH/10 % O_2/He. Evaporation of MoO_3 is observed by the decreasing intensity of the reflections at 7.43° and 8.66°. Narrow peaks between 8.25° and 8.55° are glitches due to SiO_2 background subtraction. Some initial peak shifts are observed due to the heat up from 100 to 300/350 °C.

Besides the effect of gas composition, the effect of temperature was investigated in an XRD only *operando* experiment in order to get better time resolution. Figure 8(b) shows the results of acquiring 162 diffractograms, approximately one diffractogram per minute, while heating the sample from 100 to 350 °C at 10 °C/min and staying isothermal at this temperature with a gas composition of 5 % MeOH/10 % O_2/He. Qualitatively the changes are the same as observed at 300 °C in Figure 8, with initial minor peak shifts due to the temperature increase followed by disappearance of the α-MoO_3 reflections due to evaporation. Like at 300 °C, no reflections belonging to the reduced phases $FeMoO_4$ or MoO_2 were observed at 350 °C.

The intensities of the α-MoO_3 reflections at 2θ = 7.43 and 8.66° from Figure 8(a) and (b) are shown in Figure 9(a) as function of time on stream, by setting t = 0 min when the temperature was isothermal at 300 and 350 °C, respectively. This shows an initial period of slow intensity decrease lasting about 45 and 7 min at 300 and 350 °C respectively, followed by a fast decrease until 80 and 18 min and finally flattening out and reaching the baseline intensity after 100 and 23 min at 300 and 350 °C respectively. The baseline intensity is larger than zero due to overlap with the reflections from

$Fe_2(MoO_4)_3$, particularly for the 2θ = 8.66° reflection. The change in intensity behavior can be explained by the evaporation being a function of MoO_3 content, MeOH concentration, O_2 concentration, concentration of the volatile Mo species and temperature. Initially, MoO_3 evaporates from the reactor inlet increasing the concentration of volatile Mo species in the gas, so the evaporation is slow near the center of the bed where the X-ray beam spot was placed. When all MoO_3 is removed from the inlet, the rate of evaporation at the beam spot increases and finally the rate of evaporation decreases because the particles shrink and disappear. Since the MeOH and O_2 concentrations and the temperature are close to constant throughout the catalyst bed, the rate of volatilization only depends on the concentration of the volatile Mo species in the gas phase, which evolves with time on stream. This behavior was also somewhat observed by the intensity change of features D1 and D3 by XANES (see Figure 6). The maximum rates of intensity change are $-0.97 \cdot 10^{-3}$ min^{-1} and $-0.34 \cdot 10^{-3}$ min^{-1} for the 2θ = 7.43° reflection and $-1.56 \cdot 10^{-3}$ min^{-1} and $-0.55 \cdot 10^{-3}$ min^{-1} for the 2θ = 8.66° reflection at 350 and 300 °C respectively. Thus, the rate of MoO_3 volatilization is about 3 times higher at 350 °C compared to 300 °C, but the overall trend appears to be the same. Additionally, the 2θ = 8.66° reflection, which also belongs to the $Fe_2(MoO_4)_3$ phase, has a slow intensity decline from 25 min to the end of the experiment at 350 °C. This is an indication that $Fe_2(MoO_4)_3$ is reduced to $FeMoO_4$, as observed in the *ex situ* experiments with time on stream between 100 and 600 h [19]. The time needed to positively identify $FeMoO_4$ by *operando* XRD is beyond the possibilities for a synchrotron experiment. The corresponding MS traces for *m*/*z* = 31 (MeOH), 29 (formaldehyde, corrected for MeOH) and 18 (water) are shown in Figure 9(b) showing a decrease in catalytic activity, by increasing MeOH concentration and decreasing water and formaldehyde concentrations, as the MoO_3 evaporates.

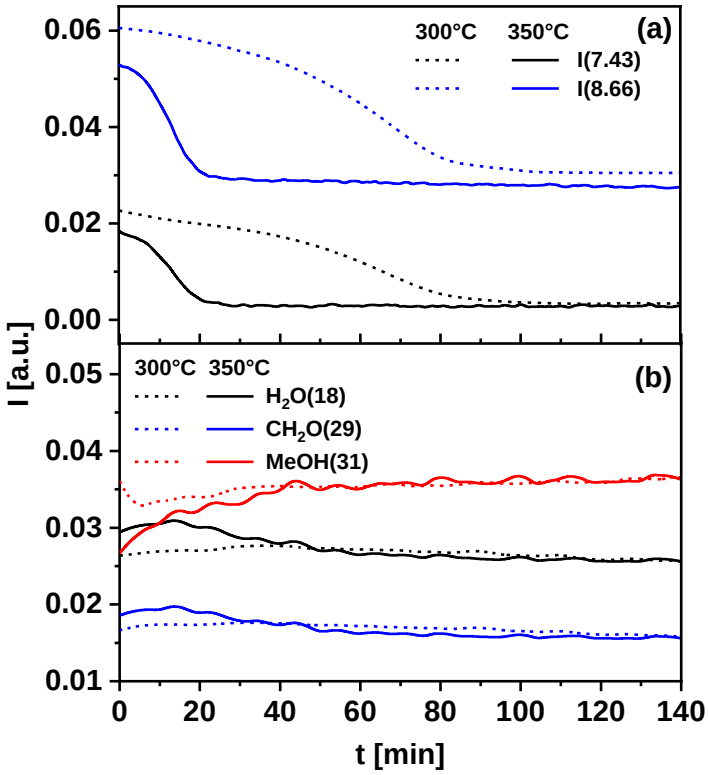

Figure 9: (a) Intensity of the α-MoO_3 reflections at 2θ = 7.43 and 8.66 as function of time under reaction conditions of 5 % MeOH/10 % O_2/He at 300 and 350 °C. t = 0 min is defined as the time when temperature was stable. Due to overlap with $Fe_2(MoO_4)_3$ reflections, zero intensity is never reached. (b) Corresponding MS traces for m/z = 31 (MeOH), 29 (formaldehyde, corrected for MeOH) and 18 (water).

3.3 Final State of the Catalyst

The final state of the catalyst was measured after cooling down to 100 °C in the reaction atmosphere, see Figure 10(a), (b) and (c). The increase in the pre-edge feature A and decrease in XANES feature B are pronounced. The difference spectra obtained by subtracting the MoO_3 reference spectrum are also shown. It can be clearly observed that MoO_3 evaporated completely and even after cooling to 100 °C, no measurable change in the characteristic peak intensity has been observed, showing only the presence of $Fe_2(MoO_4)_3$. Additionally, the intensity of the first Mo-O peak in the Fourier transformed spectrum increased, with a corresponding increase in CN of this shell from 4.7 to 5.2. The Mo-O contribution at 1.77 Å corresponds only to the tetrahedral arrangement. Thus, a relative increase in the CN at 1.77 Å shows stronger tetrahedral nature, corresponding to a larger proportion of $Fe_2(MoO_4)_3$. The Debye-Waller factor of the Mo-O contributions at 2.04 and 2.36 Å was very high, corresponding to octahedral coordination, showing higher disorder and trace concentration. Also,

Mo-Fe and Mo-Mo shells could be fitted, but the Mo-Mo distance decreased from 3.74 to 3.66 Å, as would be expected for MoO_3 evaporation due to the shorter Mo-Mo distance in $Fe_2(MoO_4)_3$ than MoO_3 (cf. Table 1). This confirms that the changes are not just an effect of the *operando* experiments (e.g. due to temperature), but are maintained after cooling the sample. The corresponding fitting in R space is given in the Supplementary Information (Figure S7).

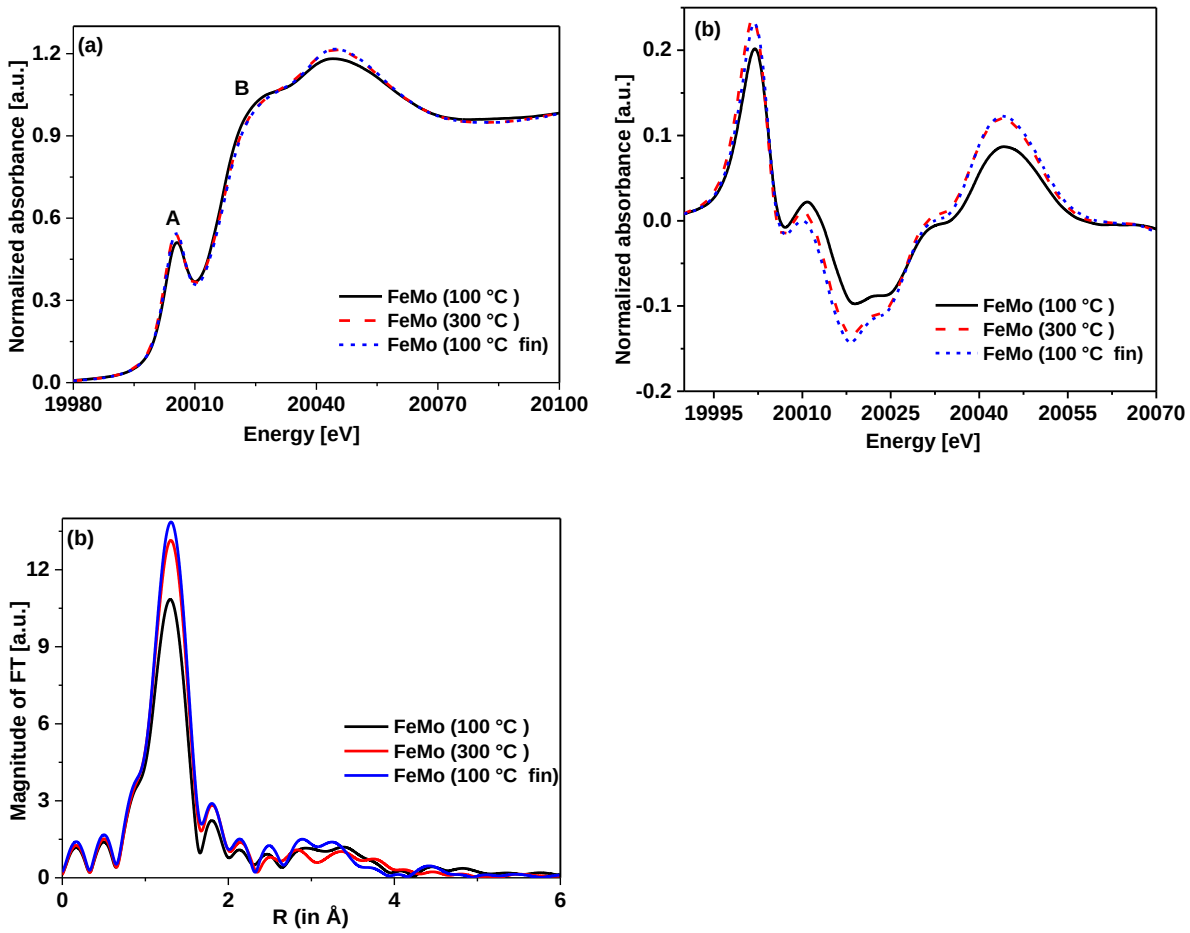

Figure 10: XANES (a), corresponding difference spectra obtained by subtracting a MoO_3 reference spectrum from given spectra (b) and k^3-weighted Fourier transformed EXAFS spectra (c) of the first spectrum (100 °C), last spectrum at 300 °C and final spectrum after cool down (100 °C) acquired under reaction conditions 5 % MeOH/10 % O_2/He.

Table 3: EXAFS fitting results of the spectrum of the final state of the catalyst after cooling to 100 °C as shown in Figure 10 (b). S_0^2 was fixed to 0.82(0.05) as determined from Mo foil. $\Delta E_0 = 2.3\ (1.3)$ and $\chi_v^2 = 70$

Path	R [Å]	CN	σ^2
Mo-O_1	1.77	5.2±0.3	0.0027
Mo-O_2	2.04/2.36	1/1	0.0135
Mo-Fe	3.48	1	0.0059
Mo-Mo	3.66	1	0.0059

3.4 STRUCTURAL CHANGES FOLLOWED WITH RAMAN SPECTROSCOPY

Operando Raman spectroscopy was used to monitor changes of the structure and the phase composition of the FeMo catalyst when subjected to reaction conditions, to complement the XAS/XRD measurements. The Raman spectra of the freshly synthesized catalyst and the catalyst after calcination at 400 °C for 2 h in flowing 10 % O_2/N_2 are shown in Figure 11. The observed bands show that the fresh catalysts consist of a mixture of $Fe_2(MoO_4)_3$, α-MoO_3 and hexagonal h-MoO_3. The latter phase is a metastable polymorph of MoO_3, containing different amounts of either H_2O and/or NH_3 in the hexagonal channels of the crystal lattice [35]. The amounts of remaining H_2O and NH_3 in the structure depend on the exact conditions during decomposition of the synthesis precursor, ammonium heptamolybdate in this case.

The tetrahedral and octahedral MoO_x units of $Fe_2(MoO_4)_3$ and α-MoO_3 respectively results in different and characteristic Raman bands [36,37]. The tetrahedral MoO_4 units of $Fe_2(MoO_4)_3$ are isolated from each other and the corresponding Raman spectrum is characterized by a triple peak feature at 987, 967 and 932 cm^{-1}, which originates from symmetric stretches of terminal Mo=O bonds of three distinct MoO_4 units [37]. The two bands at 781 and 821 cm^{-1} correspond to their asymmetric stretching vibrations [37]. A broad feature around 350 cm^{-1} originates from overlaying bands corresponding to bending modes of the MoO_4 units.

Raman bands characteristic for α-MoO_3 are found at 291 and 992 cm^{-1} (bending and stretching vibration of terminal Mo=O bond), 664 (bridging Mo-O-Mo bond that connects MoO_6 octahedra) and 819 cm^{-1} (Mo-O-Mo vibration). Bands related to lattice mode vibrations of α-MoO_3 are observed at 156, 115 and 109 cm^{-1} [38].

In a mixture of $Fe_2(MoO_4)_3$ and α-MoO_3, the $Fe_2(MoO_4)_3$ band at 987 cm^{-1} is visible as a shoulder underlying the more dominant α-MoO_3 band at 992 cm^{-1}. The $Fe_2(MoO_4)_3$ band at 821 cm^{-1} contributes

with a low intensity compared to the α-MoO_3 band at 819 cm^{-1}. Thus, the latter feature is only related to the α-MoO_3 phase in the following.

Similar to α-MoO_3, the characteristic structural motif in h-MoO_3 consists of pairs of edge-sharing distorted MoO_6 octahedra. Atuchin et al. [39] found Raman bands at 978, 697, 492, 398, 250 and 134 cm^{-1} and a characteristic triple peak at 912, 901 and 880 cm^{-1}. In this study, only one well-distinguishable peak at 896 cm^{-1} was observed in this range and no band at 978 cm^{-1} was observed. This is likely due to overlap with the dominating band from $Fe_2(MoO_4)_3$ at 967 cm^{-1}. Raman bands between 880 and 978 cm^{-1} are attributed to vibrations of the terminal Mo=O bond. Bands located at 398, 492 and 697 cm^{-1} are related to O-Mo-O vibrations. One possible explanation for the single Raman band observed at 896 cm^{-1} is partial decomposition and recrystallization of the h-MoO_3 structure under the hydrothermal synthesis conditions.

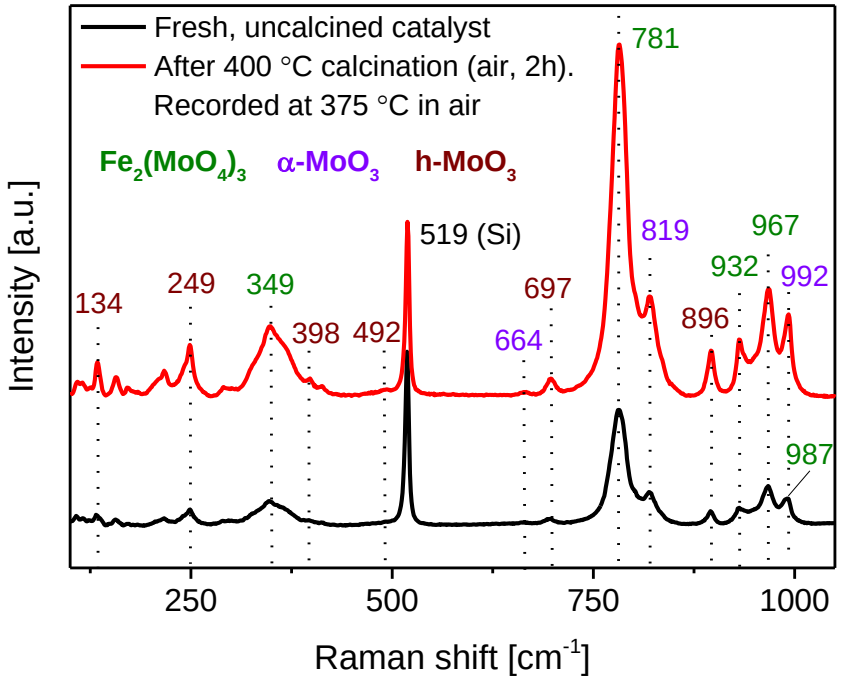

Figure 11: Raman spectra of the fresh and calcined FeMo catalyst showing that it consists of a mixture of $Fe_2(MoO_4)_3$, α-MoO_3 and hexagonal MoO_3. Calcination treatment was 2 h at 400 °C in air, subsequent cool down to 375 °C. The spectrum of the calcined catalyst was recorded at 375 °C. Spectra were baseline subtracted and normalized to the Si band at 519 cm^{-1}.

After calcination, bands related to $Fe_2(MoO_4)_3$ and h-MoO_3 increased in intensity, indicating a continuing crystallization of the catalyst material. Additionally, Raman bands assigned to the thermodynamically stable α-MoO_3 phase (992, 819, and 664 cm^{-1}) also increased in intensity. The fact that Raman bands assigned to h-MoO_3 (e.g. 896, 697, 249 cm^{-1}) do not diminish after calcination, indicates that hydrothermal synthesis of the FeMo catalyst may lead to the co-existence of an amorphous MoO_3 and a crystalline h-MoO_3 phase. Calcination then dominantly converts the amorphous phase into the thermodynamically more stable α-MoO_3 phase.

Raman spectra were continuously recorded with a short acquisition time during the initial exposure to reaction conditions of 5 % MeOH/9.5 % O_2/N_2 at 375 °C (see Figure 12). Introduction of MeOH causes an immediate, significant decrease in the signal intensity of all Raman bands (comparison of spectrum (a) to (b) in Figure 12). The most likely explanation is a disturbance of the resonance Raman effect [40]. Raman bands related to the less stable h-MoO_3 phase completely disappeared, no characteristic bands at 895, 692 or 244 cm^{-1} were observed after a few minutes on stream (Figure 12 (c-e)), while Raman bands assigned to α-MoO_3 (991, 818, 659, 280 cm^{-1}) increased in intensity. This suggests that the presence of MeOH facilitates the conversion of h-MoO_3 into the thermodynamically stable α-MoO_3 phase [35,41] and that the system stabilized within the first 3-4 min on stream.

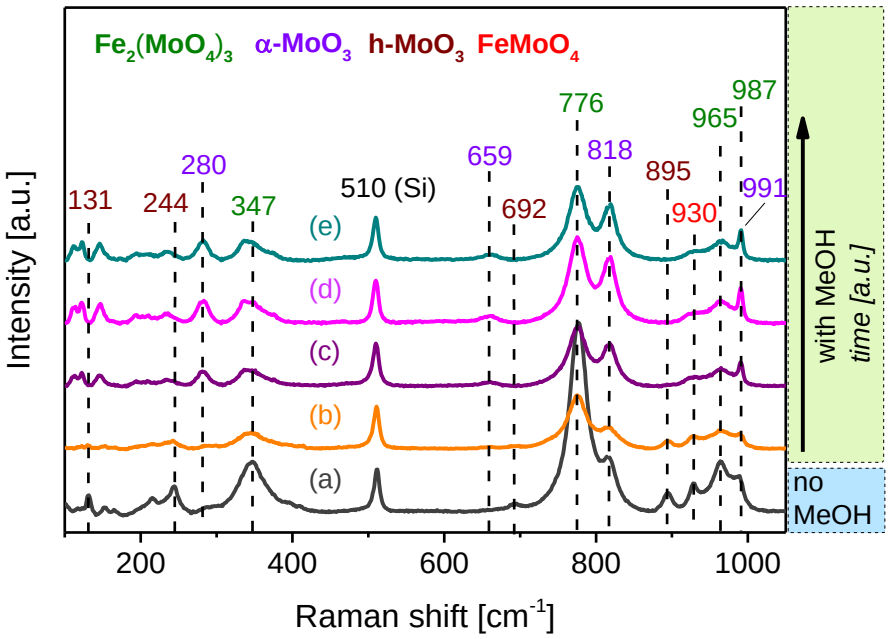

Figure 12: Raman spectra recorded before in He atmosphere (a) and during the initial period under reaction conditions of 5 % MeOH/9.5 % O_2/N_2 at 375 °C (b-e). Approximate time difference between Raman spectra (b-e) is one minute. Spectra were baseline subtracted and normalized to the Si band at 510 cm^{-1}.

Observation of the catalyst under reaction conditions for a period of 10 h on stream (Figure 13) show α-MoO_3 Raman bands decreasing and eventually disappearing during the first 5 to 7 h on stream. From 7 to 10 h on stream, the Raman spectra show only well-defined bands for $Fe_2(MoO_4)_3$. Remaining low intensity Raman bands assigned to α-MoO_3 may be caused by a surface layer structure of MoO_x.

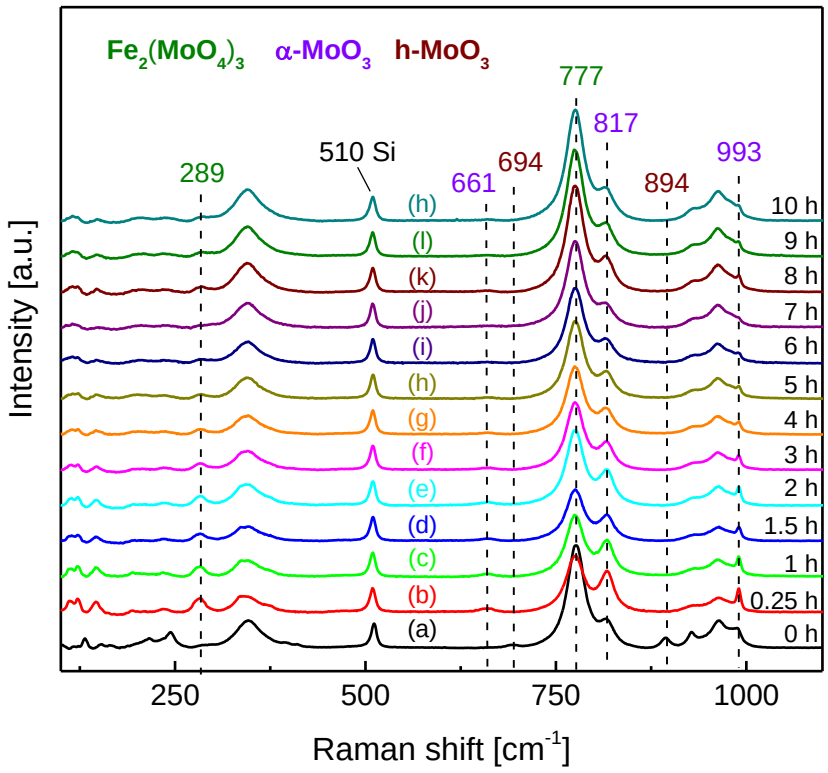

Figure 13: Raman spectra recorded before catalytic reaction at 375 °C in pure air (a) and after different times on stream under reaction conditions (b-h). Spectra were baseline subtracted and normalized to the Si band at 510 cm^{-1}.

The spectra in Figure 13 were de-convoluted into different spectral components using Voigt curves for peak fitting as recommended for inorganic, ceramic materials [42]. The spectra were normalized to the 776 cm^{-1} peak of $Fe_2(MoO_4)_3$ so the relative change in intensity of the α-MoO_3 bands at 660 and 990 cm^{-1} can be followed (for details see the Supplementary Information Section 3). The intensity of the α-MoO_3 bands and the correspondingly measured MeOH conversion are plotted in Figure 14. Within the first ten hours, there is a clear decrease in the intensity of the Raman bands assigned to the α-MoO_3 phase. The decline is correlated with a decrease in MeOH conversion from 85 to 67 %. This additionally demonstrates that the catalyst deactivates as MoO_3 evaporates. Supplementary Information Figure S9 shows the simultaneous increase of Raman bands assigned to $Fe_2(MoO_4)_3$, when normalizing the spectra to the Si band.

The rate of MoO_3 evaporation in the *operando* Raman experiments was much lower than in the *operando* XAS/XRD experiments, but similar to the previous *ex situ* observations where all MoO_3 had

evaporated after 10 h on stream, according to Raman spectroscopy and XRD [19]. This is likely because the catalyst particle size used in the *operando* Raman experiment is similar to the particle size used in the long term stability experiments [19], while the particle size used for *operando* XAS/XRD is much smaller, as discussed in Section 3.2. Studies on whole, industrial iron molybdate/molybdenum oxide catalyst pellets showed that evaporation of MoO_3 is strongly diffusion limited [20], which explains the difference observed between different methods, using different particle sizes in this study.

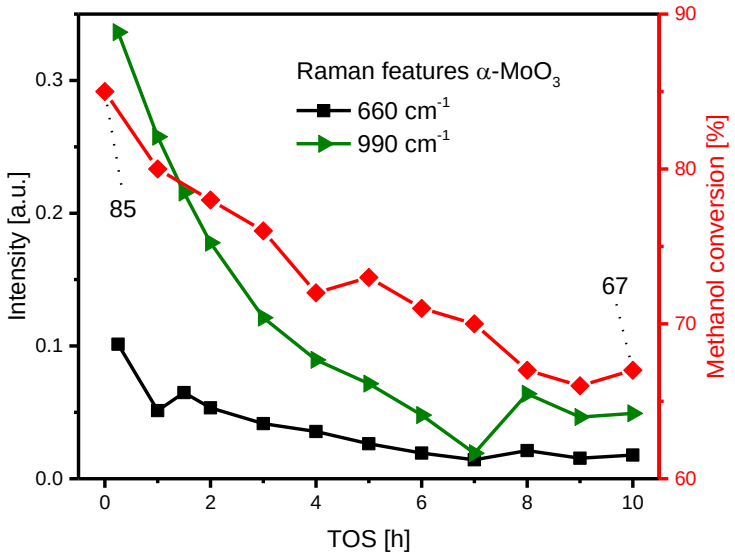

Figure 14: Change of intensity of characteristic Raman features assigned to α-MoO_3 at 660 and 990 cm^{-1} as a function of time on stream, together with the MeOH conversion. Reaction conditions 375 °C with 5 % MeOH/9.5 % O_2/N_2. Spectra were background subtracted and normalized against the Raman band at 776 cm^{-1} which is solely assigned to $Fe_2(MoO_4)_3$. Thus, changes to the bands related to α-MoO_3 occur relative to $Fe_2(MoO_4)_3$. Further information on the spectra fitting are provided in the Supporting Information (section 3).

4 Conclusions

Correlative and *operando* XAS, XRD and Raman spectroscopy uncovered that the industrial type FeMo catalyst undergoes strong structural changes during its evolution with time on stream for selective oxidation of methanol to formaldehyde. The significant changes occurred due to the volatilization and evaporation of MoO_3. For small particles, a concurrent decrease in catalytic activity was observed. By utilizing the characteristic XANES features of $Fe_2(MoO_4)_3$ and MoO_3, the amount of evaporated MoO_3 was quantified by normalized difference edge analysis. The rate of volatilization was

highly dependent on the reaction conditions with increasing rate at higher MeOH concentration, lower O_2 concentration and increasing temperature. At 300 °C the rate of MoO_3 volatilization increased by 67 % upon decreasing of the O_2 concentration from 10 to 5 % (with 5 % MeOH). Increasing the MeOH concentration from 5 to 9.5 % at 5 % O_2 further accelerated the volatilization by a factor of two. Increasing the temperature from 300 to 350 °C at 5 % MeOH and 10 % O_2 increased the rate of volatilization by about a factor of three. The $Fe_2(MoO_4)_3$ phase appeared stable within the time frame of the experiments, but at 350 °C some indication of Mo volatilization from $Fe_2(MoO_4)_3$, forming $FeMoO_4$, was additionally derived from XRD, after all MoO_3 had evaporated. This shows that MoO_3 cannot act as a replenishing reservoir for molybdenum lost from $Fe_2(MoO_4)_3$.

A significant effect of catalyst particle size was observed. The rate of volatilization in the *operando* Raman experiments, where a 150 to 300 µm sieve fraction was used, was much lower than in the *operando* XAS/XRD experiments, where finely ground particles mixed with SiO_2 (100 to 150 µm) were used. This supports earlier conclusions that the evaporation is limited by diffusion of volatile Mo compounds out of the catalyst particles.

Even though the MoO_3 volatilize it plays an important role in the industrial catalyst for mechanical strength of the pellets and as sacrificial molybdenum oxide, saturating the gas phase with volatile molybdenum compounds, minimizing the volatilization of Mo from $Fe_2(MoO_4)_3$, which would form the less selective phases $FeMoO_4$ and Fe_2O_3 with time on stream.

Understanding the effects of reaction conditions and catalyst structure on activity, selectivity and stability is highly important for rational optimization of both catalyst formulations and reaction conditions. This work is a step in this direction for the FeMo catalyst used for selective oxidation of methanol, but is also of importance for the use of molybdenum oxide based catalysts in general.

ACKNOWLEDGEMENTS

We thank the Independent Research Fund Denmark for the financial support (grant no: DFF – 4184-00336). We are grateful to ESRF for providing beamtime at the Swiss- Norwegian-beamline BM31 for combined XAS/XRD studies and, in particular, to Dr. Hermann Emerich and Dr. Wouter van Beek for their help and technical support during XAS experiments. We thank Marc-André Serrer (KIT) for his support during the beamtime. We also thank KIT's synchrotron radiation source (operated by KIT-IBPT) for *ex situ* XAS measurements conducted at the CAT-ACT beamline.

REFERENCES

[1] G. Reuss, W. Disteldorf, A. O. Gamer, A. Hilt, in *Ullmann's Encycl. Ind. Chem.*, Wiley-VCH Verlag GmbH & Co. KGaA, **2000**.

[2] M. Carbucicchio, F. Trifirò, *J. Catal.* **1976**, *45*, 77–85.

[3] G. Alessandrini, L. Cairati, P. Forzatti, P. L. Villa, F. Trifirò, *J. Less-Common Met.* **1977**, *54*, 373–386.

[4] A. P. V. Soares, M. F. Portela, A. Kiennemann, L. Hilaire, *Chem. Eng. Sci.* **2003**, *58*, 1315–1322.

[5] M. Bowker, R. Holroyd, A. Elliott, P. Morrall, A. Alouche, C. Entwistle, A. Toerncrona, *Catal. Letters* **2002**, *83*, 165–176.

[6] B. I. Popov, V. N. Bibin, G. K. Boreskov, *Kinet. i Katal.* **1976**, *17*, 371–377.

[7] A. Andersson, M. Hernelind, O. Augustsson, *Catal. Today* **2006**, *112*, 40–44.

[8] B. R. Yeo, G. J. F. Pudge, K. G. Bugler, A. V. Rushby, S. Kondrat, J. Bartley, S. Golunski, S. H. Taylor, E. Gibson, P. P. Wells, et al., *Surf. Sci.* **2016**, *648*, 163–169.

[9] A. M. Beale, S. D. M. Jacques, E. Sacaliuc-Parvalescu, M. G. O'Brien, P. Barnes, B. M. Weckhuysen, *Appl. Catal. A Gen.* **2009**, *363*, 143–152.

[10] C. Brookes, P. P. Wells, N. Dimitratos, W. Jones, E. K. Gibson, D. J. Morgan, G. Cibin, C. Nicklin, D. Mora-Fonz, D. O. Scanlon, et al., *J. Phys. Chem. C* **2014**, *118*, 26155–26161.

[11] C. Brookes, M. Bowker, E. K. Gibson, D. Gianolio, K. M. H. Mohammed, S. Parry, S. M. Rogers, I. P. Silverwood, P. P. Wells, *Catal. Sci. Technol.* **2016**, *6*, 722–730.

[12] C. Brookes, P. P. Wells, G. Cibin, N. Dimitratos, W. Jones, D. J. Morgan, M. Bowker, *ACS*

Catal. **2014**, *4*, 243–250.

[13] C. Brookes, M. Bowker, P. Wells, *Catalysts* **2016**, *6*, 92.

[14] A. P. V. Soares, M. F. Portela, A. Kiennemann, L. Hilaire, *Chem. Eng. Sci.* **2003**, *58*, 1315–1322.

[15] M. G. G. O'Brien, A. M. M. Beale, S. D. M. D. M. Jacques, M. Di Michiel, B. M. M. Weckhuysen, M. Di Michiel, B. M. M. Weckhuysen, M. Di Michiel, B. M. M. Weckhuysen, *ChemCatChem* **2009**, *1*, 99–102.

[16] M. G. O'Brien, A. M. Beale, S. D. M. Jacques, B. M. Weckhuysen, *Top. Catal.* **2009**, *52*, 1400–1409.

[17] M. G. O'Brien, A. M. Beale, S. D. M. Jacques, T. Buslaps, V. Honkimaki, B. M. Weckhuysen, *J. Phys. Chem. C* **2009**, *113*, 4890–4897.

[18] M. G. O'Brien, A. M. Beale, S. D. M. Jacques, M. Di Michiel, B. M. Weckhuysen, *Appl. Catal. A Gen.* **2011**, *391*, 468–476.

[19] K. V. Raun, L. F. Lundegaard, J. Chevallier, P. Beato, C. C. Appel, K. Nielsen, M. Thorhauge, A. D. Jensen, M. Høj, *Catal. Sci. Technol.* **2018**, *8*, 4626–4637.

[20] K. V. Raun, J. Johannessen, K. McCormack, C. C. Appel, S. Baier, M. Thorhauge, M. Høj, A. D. Jensen, *Chem. Eng. J.* **2019**, *361*, 1285–1295.

[21] W. van Beek, O. V Safonova, G. Wiker, H. Emerich, *Phase Transitions* **2011**, *84*, 726–732.

[22] B. Ravel, M. Newville, *J. Synchrotron Rad.* **2005**, *12*, 537–541.

[23] P. Villars, K. Cenzual, Eds. , "MoO3 Crystal Structure: Datasheet from 'PAULING FILE Multinaries Edition – 2012' in SpringerMaterials," can be found under https://materials.springer.com/isp/crystallographic/docs/sd_0530932, **2012**.

[24] P. Villars, K. Cenzual, Eds. , "Fe2(MoO4)3 (Fe2[MoO4]3 rt) Crystal Structure: Datasheet from 'PAULING FILE Multinaries Edition – 2012' in SpringerMaterials," can be found under https://materials.springer.com/isp/crystallographic/docs/sd_0376289, **2012**.

[25] J. J. Rehr, J. J. Kas, F. D. Vila, M. P. Prange, K. Jorissen, *Phys. Chem. Chem Phys.* **2010**, *12*, 5503–5513.

[26] J.-D. Grunwaldt, M. Caravati, S. Hannemann, A. Baiker, *Phys. Chem. Chem. Phys.* **2004**, *6*, 3037–3047.

[27] C. G. Schroer, J.-D. Grunwaldt, in *In-Situ Charact. Heterog. Catal.*, John Wiley & Sons, Inc., **2013**, pp. 49–73.

[28] J.-D. Grunwaldt, N. van Vegten, A. Baiker, *Chem. Commun.* **2007**, 4635–4637.

[29] P. Beato, E. Schachtl, K. Barbera, F. Bonino, S. Bordiga, *Catal. Today* **2013**, *205*, 128–133.

[30] M. R. Antonio, R. G. Teller, D. R. Sandstrom, M. Mehicic, J. F. Brazdil, *J. Phys. Chem.* **1988**, *92*, 2939–2944.

[31] A. M. Beale, G. Sankar, *Chem. Mater.* **2003**, *15*, 146–153.

[32] P. R. Huang, Y. He, C. Cao, Z. H. Lu, *Sci. Rep.* **2014**, *4*, 1–7.

[33] L. S. Kau, D. J. Spira-Solomon, J. E. Penner-Hahn, K. O. Hodgson, E. I. Solomon, *J. Am. Chem. Soc.* **1987**, *109*, 6433–6442.

[34] A. Gaur, B. D. Shrivastava, S. K. Joshi, *J. Phys. Conf. Ser.* **2009**, *190*, 12084.

[35] H. J. Lunk, H. Hartl, M. A. Hartl, M. J. G. Fait, I. G. Shenderovich, M. Feist, T. A. Frisk, L. L. Daemen, D. Mauder, R. Eckelt, et al., *Inorg. Chem.* **2010**, *49*, 9400–9408.

[36] K. Routray, W. Zhou, C. J. Kiely, W. Grünert, I. E. Wachs, *J. Catal.* **2010**, *275*, 84–98.

[37] H. Tian, I. E. Wachs, L. E. Briand, *J. Phys. Chem. B* **2005**, *109*, 23491–23499.

[38] G. Mestl, T. K. K. Srinivasan, H. Knöml;zinger, *Langmuir* **1995**, *11*, 3795–3804.

[39] V. V. Atuchin, T. A. Gavrilova, V. G. Kostrovsky, L. D. Pokrovsky, I. B. Troitskaia, *Inorg. Mater.* **2008**, *44*, 622–627.

[40] M. Dieterle, G. Weinberg, G. Mestl, *Phys. Chem. Chem. Phys.* **2002**, *4*, 812–821.

[41] A. Chithambararaj, A. C. Bose, *J. Alloys Compd.* **2011**, *509*, 8105–8110.

[42] X. Yuan, R. A. Mayanovic, *Appl. Spectrosc.* **2017**, *71*, 2325–2338.